GEOFIZIKA VOL. 13 1996

Original scientific paper
UDC 550.341

P-wave magnitude spectra, stress drops, rupture complexities and other source parameters from broadband seismograms of three 1987 Southern California earthquakes

Diethelm Kaiser[1], *Seweryn J. Duda*[1] *and Dipak K. Chowdhury*[2]

[1]Institute of Geophysics, Hamburg University, 20146 Hamburg, F. R. Germany
[2]Dept. of Geosciences, Indiana University–Purdue University at Fort Wayne, Fort Wayne, IN 46805-1499, USA

Received 1 April 1996, in final form 27 October 1996

Three large earthquakes in Southern California – the Whittier Narrows earthquake of 1 October 1987 (WN), and the Elmore Ranch (ER) and Superstition Hills (SH) earthquakes of 24 November 1987 are analyzed using broadband recordings from the Graefenberg (GRF) array. The P-wave seismograms from all stations of the array are utilized to determine the magnitude spectra of the earthquakes. The magnitude spectrum represents the velocity amplitude density spectrum at the earthquake source, scaled in magnitude units. At 1 Hz the magnitude spectra show good agreement with the NEIC m_b (5.8, 5.7, and 6.0 respectively for events WN, ER, and SH). The maximum magnitudes, however, occur at longer periods (16 s, 4.1 s, and 3.6 s, for WN, ER, and SH) and have larger values (6.3, 6.6, and 6.7 for WN, ER, and SH). Other source parameters determined from the magnitude spectra are P-wave energy, seismic moment, fault length, average stress drop, and source complexity. The magnitude spectra and the source parameters show systematic variations across the stations of the GRF array. These variations are interpreted as the effect of changes in the local geologic conditions underneath the array. The variations are smallest for the maximum spectral magnitude (with a standard deviation of less than 1%) and largest for the stress drop (average standard deviation of 40%).

Additional source parameters derived from the magnitude spectra are: asperity radius, displacement across the asperity, localized stress drop, and ambient faulting stress. Significant differences in the magnitude spectra and source parameters are observed between ER and SH on one side and WN on the other. The magnitude spectra of ER and SH are much simpler in shape, as compared to WN, which in turn is characterized by a high complexity and a low average stress drop (0.1 MPa). ER appears to be the result of a smooth and simple rupture with a homogeneous stress drop. SH reveals a moderate rupture complexity.

Keywords: Magnitude spectra, earthquake source parameters, Southern California.

Spektri magnituda P valova, pad napetosti, složenost rasjedanja i drugi parametri potresnih izvora određeni analizom širokopojasnih seizmograma tri južnokalifornijska potresa iz 1987. godine

Tri velika južnokalifornijska potresa – Whittier Narrows potres od 1. listopada 1987. (WN), te Elmore Ranch (ER) i Superstition Hills (SH) od 24. studenoga 1987. – analizirana su na temelju širokopojasnih seizmograma seizmografske mreže Graefenberg (GRF). Zapisi P valova sa svih postaja mreže rabljeni su za određivanje spektara magnituda koji su reprezentativni za spektre gustoće brzine pomaka u izvoru izražene jedinicama magnitude. Na frekvenciji od 1 Hz magnitudni se spektri dobro slažu s m_b magnitudama određenim u NEIC-u (5.8, 5.7 i 6.0, redom za potrese WN, ER i SH). Maksimalna se magnituda međutim javlja na dužim periodima (16 s, 4.1 s i 3.6 s za WN, ER i SH) i većeg je iznosa (6.3, 6.6 i 6.7 za WR, ER i SH). Na osnovi magnitudnih spektara određeni su i drugi parametri seizmičkih izvora: energija P valova, seizmički moment, duljina rasjeda, prosječni pad napetosti i složenost izvora, koji unutar GRF mreže pokazuju sustavne varijacije. Te se varijacije mogu objasniti lokalnim geološkim svojstvima tla na području mreže. Najmanje su za maksimalnu spektralnu magnitudu (sa standardnom devijacijom manjom od 1%) a najveće za pad napetosti (srednja standardna devijacija od 40%).

Dodatni parametri izvora koje je bilo moguće odrediti su: polumjer »asperity« područja na rasjedu i pomak na njima, lokalizirani pad napetosti, te okolna napetost rasjedanja. Značajne razlike u spektrima magnituda i parametrima izvora vidljive su između ER i SH s jedne, i WN potresa s druge strane. Spektri magnituda ER i SH su jednostavnijeg oblika, dok oni koji se odnose na WN iskazuju veću složenost i manji prosječni pad napetosti (0.1 MPa). Čini se da je u slučaju ER došlo do jednostavnog i glatkog rasjedanja s homogenim padom napetosti. SH pokazuje umjerenu složenost rasjedanja.

Introduction

Three large earthquakes occurred in Southern California in 1987, within a time span of eight weeks. They are the Whittier Narrows earthquake (WN) of October 1, and the Elmore Ranch (ER) and Superstition Hills earthquakes (SH) on 24 November, the last being the strongest in the region since the Imperial Valley earthquake of 1979. The epicenters of these events are located within a distance of 250 km of each other. The temporal and spatial proximity of the events, particularly of the latter two, indicates an interdependence. The fact that these two events are located on a conjugate fault system characterized by intense seismicity supports such a notion (Hudnut et al., 1989; Hanks and Allen, 1989; Hamilton, 1972; and Johnson and Hutton, 1982).

The three events have been studied extensively. The studies are based mainly on the analysis of regional seismological data collected from short- and long-period seismographs, as well as from accelerographs. A special section on the Whittier Narrows earthquake (Journal of Geophysical Research, Vol. 94,

1989), and a special issue on the Elmore Ranch and Superstion Hills earthquakes (Bulletin of the Seismological Society of America, Vol. 79, 1989) have been published.

In this paper we present data obtained from the broadband seismographs at the Central Seismological Observatory of the Federal Republic of Germany at Erlangen, located at a distance of about 85° from the epicenters. We discuss the problem of extracting source parameters from the teleseismic observations, and the possibility of recognizing and quantifying individual features of the radiation process at the hypocenters. The analysis is based on the concept of magnitude spectra. The higher attenuation of S-waves, and the generally less favorable signal-to-noise ratio for these waves renders the analysis of spectral S-wave magnitudes at large epicentral distances impossible at least in the present case. Thus, in the following only spectral P-wave magnitudes are analyzed.

The magnitude spectrum is a generalization of the concept of the body wave magnitude. Customarily, a short-period and a long-period body wave magnitude is published for seismic events. The National Earthquake Information Center (NEIC) of the U.S. Geological Survey, for example, publishes short-period body wave magnitudes based on P-waves in the period range from 0.1 s–3.0 s, *i.e.* m_b is an average value over nearly 5 octaves.[1] An additional, intermediate-period body wave magnitude is also given occasionally. The body wave magnitudes of a particular earthquake constitute discrete samples of the velocity density spectrum, the samples being averages corresponding to period ranges, not always specified (Nortmann and Duda, 1982, 1983). The sampling of the spectra is strongly influenced by the passband of the seismometer-galvanometer system. Thus. *e.g.* for a short-period, WWSSN seismometer-galvanometer system which has a maximum magnification at 1 Hz and a passband between 0.79 and 1.67 Hz, the body wave magnitude is a measure of the velocity density spectrum in the frequency range 0.79–1.67 Hz (0.60–1.27 s).

In the case of a broadband seismogram, practically the whole spectrum of the arriving signal is recorded without amplitude distortion. If a set of filters, with non-overlapping bandwidths is applied to the broadband signal, bandpass seismograms are obtained from which P- (and S-) wave magnitudes of the given earthquake can be determined (Sarkar and Duda, 1985; Kaiser and Duda, 1986; and Chowdhury and Duda, 1986). Narrowing the passband to the resolvable frequency chosen for the Fourier transform, *i.e.* admitting only one Fourier component to each passband, yields a sequence of magnitudes which

---

[1] One might remind here that an ordinary piano comprises about 8 octaves. In analogy, m_b, as published by NEIC, corresponds then to a single measure of sound intensity in case keys of the piano are struck simultaneously over more than half of their range, with relative striking intensities varying from case to case. Such a measure is difficult to interpret indeed.

will constitute the P- (or S-) wave magnitude spectrum of the given earthquake. The magnitude spectrum is a quasi-continuous estimate of the velocity density spectrum of P- (or S-) waves expressed in magnitude units (Kaiser and Duda, 1988). Unlike the conventional body wave magnitudes, the magnitude spectrum represents the complete P- (or S-) wave energy radiated from the focus. The maximum of the magnitude spectrum along with the period at which the maximum occurs are thereby the most characteristic quantities of the radiated spectrum, at variance with the conventional body wave magnitudes determined at incidental periods and from unspecified ranges.

Determination of magnitude spectrum

Table 1 lists the pertinent details of the three Southern California earthquakes and the locations of the seismographs of the Gräfenberg (GRF) array belonging to the Central Seismological Observatory of the Federal Republic of Germany. The earthquake epicenters, the positions of the seismographs, and the instrument response to the ground motions are given in Figures 1a, b. The instruments have a constant amplification to ground velocity between 0.2 s and 20 s. The range of constant amplification is further extended to a longer period by inverse filtering of the spectrum of the signal; it is shown by the solid line (Fig. 1b).

Table 1. Earthquakes and stations

Earthquake parameters (from NEIC, U. S. Geological Survey)

ID	Region	Origin time						Hypocenter			m_b	M_s	M_0 (10^{17}Nm)
		year	mon	day	hr	min	s	Lat. (°N)	Long. (°W)	Depth (km)			
WN	Whittier Narrows	1987	10	01	14	42	20.0	34.060	118.080	10	5.8	5.7	8.4
ER	Elmore Ranch	1987	11	24	01	54	14.5	33.083	115.775	5	5.7	6.2	9.1
SH	Superstition Hills	1987	11	24	13	15	56.4	33.010	115.840	2	6.0	6.6	62.0

Central Seismological Observatory (GRF) – Location of Stations of Array

Station	Lat. (°N)	Long. (°E)	Altitude (m)	Station	Lat. (°N)	Long. (°E)	Altitude (m)	Station	Lat. (°N)	Long. (°E)	Altitude (m)
A1	49.692	11.222	500	B1	49.392	11.654	494	C1	48.996	11.522	512
A2	49.655	11.360	512	B2	49.271	11.669	552	C2	48.868	11.375	445
A3	49.762	11.319	455	B3	49.344	11.806	517	C3	48.890	11.585	438
A4	49.565	11.436	503	B4	49.469	11.561	507	C4	49.087	11.527	503
				B5	49.111	11.679	525				

Figures 2a, b, c (top) show the broadband P-wave records of the three earthquakes on the vertical component seismograph at station A1 (center of A-subarray) of GRF. The signals show little similarity. In the frequency do-

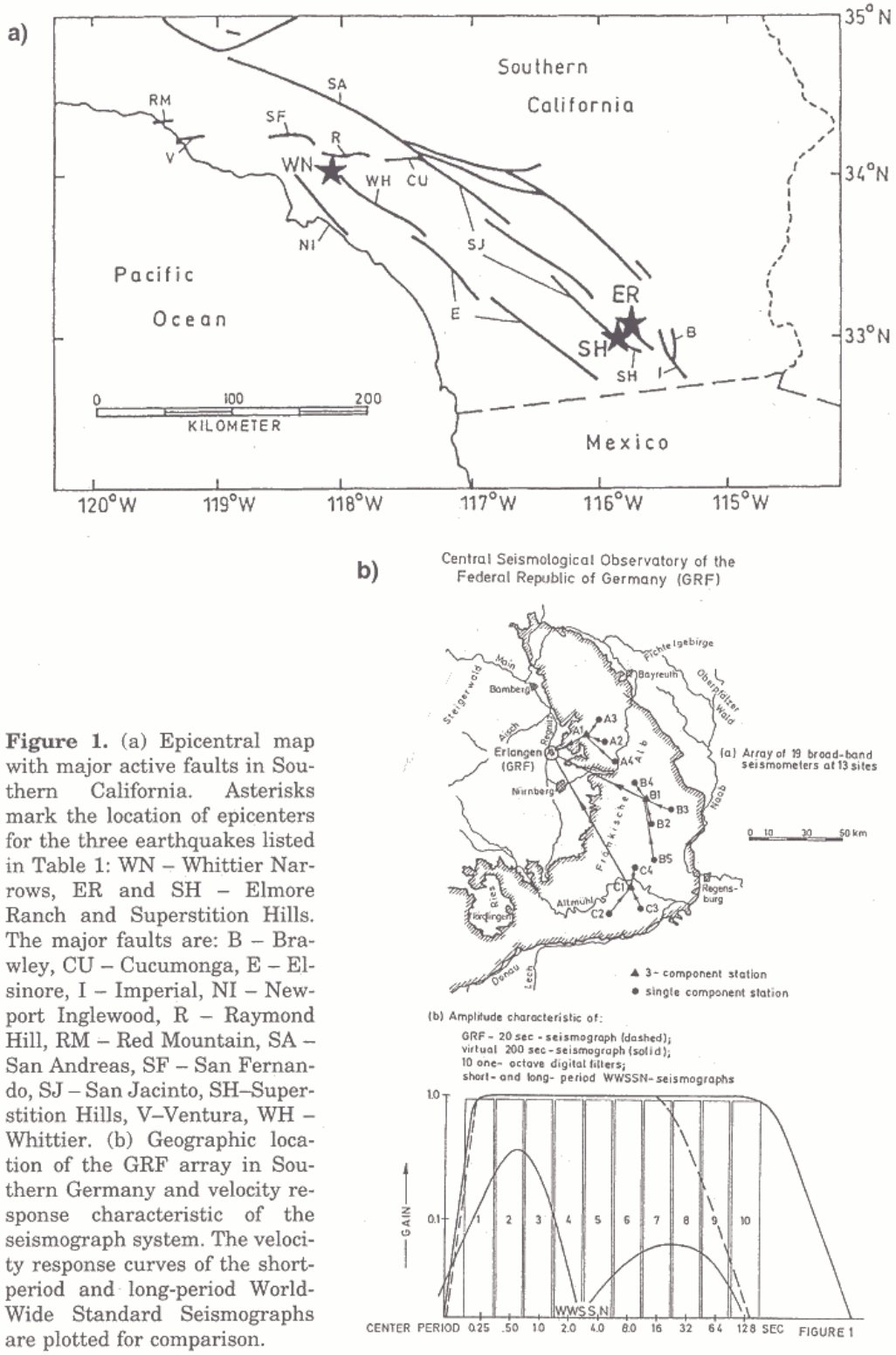

Figure 1. (a) Epicentral map with major active faults in Southern California. Asterisks mark the location of epicenters for the three earthquakes listed in Table 1: WN – Whittier Narrows, ER and SH – Elmore Ranch and Superstition Hills. The major faults are: B – Brawley, CU – Cucumonga, E – Elsinore, I – Imperial, NI – Newport Inglewood, R – Raymond Hill, RM – Red Mountain, SA – San Andreas, SF – San Fernando, SJ – San Jacinto, SH–Superstition Hills, V–Ventura, WH – Whittier. (b) Geographic location of the GRF array in Southern Germany and velocity response characteristic of the seismograph system. The velocity response curves of the short-period and long-period World-Wide Standard Seismographs are plotted for comparison.

main, however, the Elmore Ranch and the Superstition Hills earthquakes reveal a high degree of congruence, whereas the spectrum of the Whittier Narrows (WN) earthquake is different. The feature is to be analyzed in the later part of the paper.

Two factors are taken into consideration when selecting the length of the time window of 102.4 s (see Fig. 2) for the Fourier transform of the signals. First, the window must be sufficiently long to yield a stable corner period. Secondly, the window length should be the same for the earthquakes investigated (Båth, 1974). Kaiser and Duda (1988) have shown that the corner period depends on the window length, generally increasing asymptotically with the length. It was found that a stable value of the corner period is obtained when the window length is at least six times the corner period. The surface- and core-reflected phases that follow the P-waves (*e.g.* pP, sP, PcP) have little influence on the P-wave spectrum (Tucker and Brune, 1977). Based on prior experience (Kaiser and Duda, 1988), a window length of 102.4 s (corresponding to 2048 sample points), starting with the onset of P-wave, is selected. Prior to the Fourier transform a 10% cosine tapering function is used at both ends of the windowed signal. This tapering starts before the P-onset. The spectrum is corrected for the instrument response for periods between 20 and 102.4 s by dividing the spectrum by the instrument response. In order to obtain the velocity-amplitude density spectrum radiated from the source, each Fourier component is compensated for losses along the ray path through the use of the magnitude calibrating function of Nortmann and Duda (1983). The function is a generalization of Gutenberg and Richter's (1956) calibration function, and depends not only on epicentral distance and focal depth, but on the period of the wave as well. The magnitude calibrating function is based on generally accepted velocity- and Q-models of the earth (Nortmann and Duda 1982, 1983). The corrected spectrum which has been compensated for the propagation losses (both geometric and anelastic attenuation) and the instrument response, is a measure of the total seismic energy radiated from the hypocenter; it is termed magnitude spectrum.

The magnitude spectra of the three events are shown in Figures 2a, b, c (bottom). In all cases the signal-to-noise ratio is low for periods longer than 20 s due to a decrease in radiated energy at longer periods, and a simultaneous increase in the long-period noise. The increased noise is due to the combined effect of long-period atmospheric noise (Berckhemer, 1971; Savino et al. 1972), as well as instrumental and computational noise. The signal-to-noise ratio is again low around the 4 s period, where the effect of oceanic microseisms is strong. However, over most of the period range utilized the signal-to-noise ratio is larger than half an order of magnitude, and the magnitude spectrum does not appear to be perturbed by the noise. At periods shorter than about 0.6 s the local microseismic noise renders an unacceptable signal-to-noise ratio. Thus, the magnitude spectra are considered only for periods between 0.6 and 20 s (dashed lines in Fig. 2).

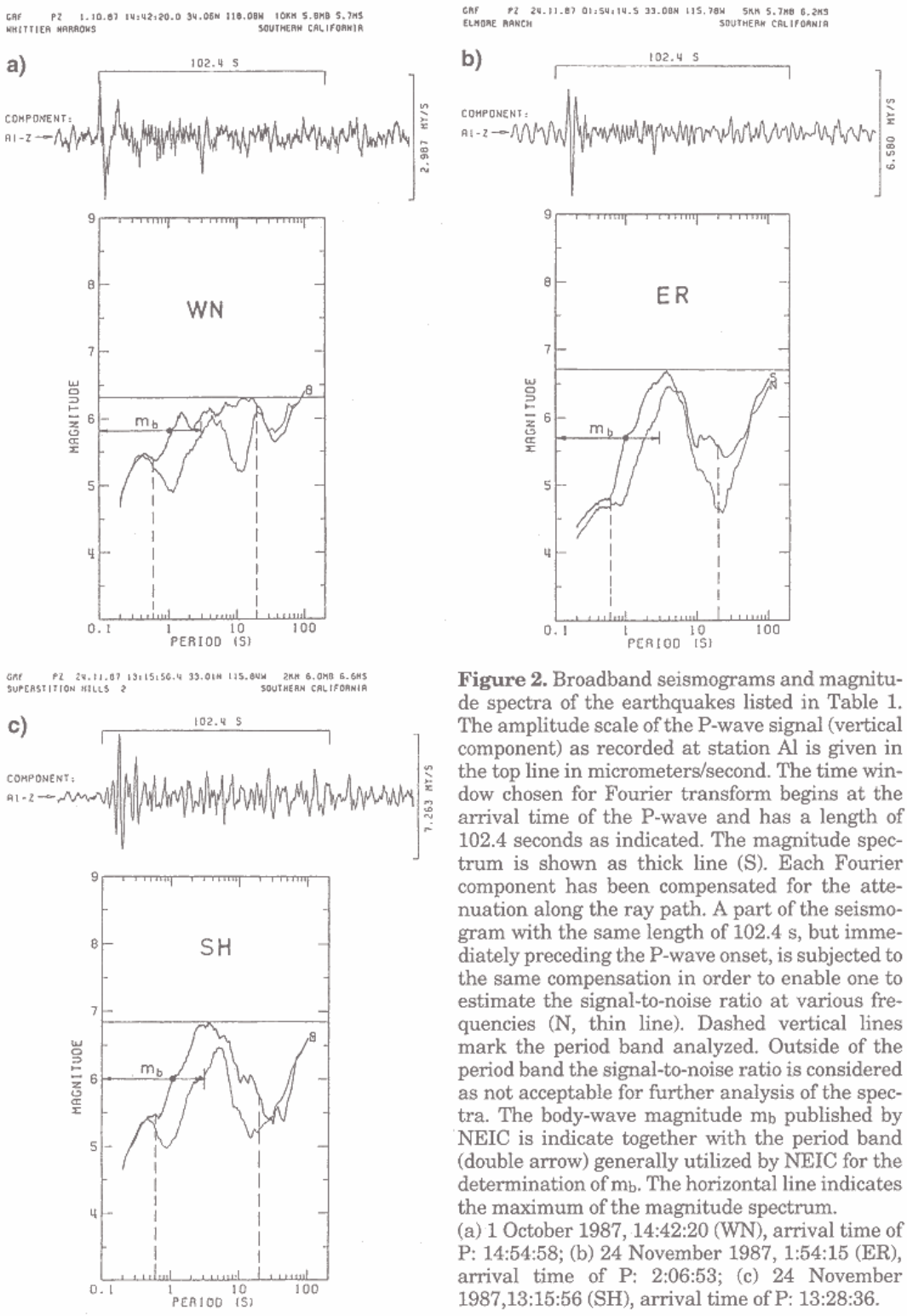

Figure 2. Broadband seismograms and magnitude spectra of the earthquakes listed in Table 1. The amplitude scale of the P-wave signal (vertical component) as recorded at station Al is given in the top line in micrometers/second. The time window chosen for Fourier transform begins at the arrival time of the P-wave and has a length of 102.4 seconds as indicated. The magnitude spectrum is shown as thick line (S). Each Fourier component has been compensated for the attenuation along the ray path. A part of the seismogram with the same length of 102.4 s, but immediately preceding the P-wave onset, is subjected to the same compensation in order to enable one to estimate the signal-to-noise ratio at various frequencies (N, thin line). Dashed vertical lines mark the period band analyzed. Outside of the period band the signal-to-noise ratio is considered as not acceptable for further analysis of the spectra. The body-wave magnitude m_b published by NEIC is indicate together with the period band (double arrow) generally utilized by NEIC for the determination of m_b. The horizontal line indicates the maximum of the magnitude spectrum.
(a) 1 October 1987, 14:42:20 (WN), arrival time of P: 14:54:58; (b) 24 November 1987, 1:54:15 (ER), arrival time of P: 2:06:53; (c) 24 November 1987,13:15:56 (SH), arrival time of P: 13:28:36.

Inspection of the magnitude spectra of the three events indicate that for the Elmor Ranch and Superstition Hills earthquakes the spectra are relatively simple in shape. The magnitude spectrum of the Whittier Narrows earthquake on the other hand is broad and complex, with a number of secondary maxima. In all three cases, the values of the magnitude spectra at 1 s period agree well with the body wave magnitudes (m_b) determined by NEIC, respectively. In each case however, the maximum magnitude $\hat{m}_f$ of the earthquake occurs at periods greater than those used by NEIC to determine m_b. The maximum magnitude is indicated in the plot by a horizontal line. The maximum magnitude $\hat{m}_f$ together with the period at which it occurs, is considered to be generally more representative of the strength of the earthquakes than m_b.

The broadband records of the P-wave and the magnitude spectra for the remaining stations of the array (A2–C4) (Table 1) are shown in Figures 3a, b, c. Only minor differences exist in the magnitude spectra recorded at the 13 sites of the array for each of the three events. The maximum magnitudes are remarkably stable, with standard deviations of less than 0.1 (column 3, Table 2). The corner periods, T_0, at which the maximum magnitudes $\hat{m}_f$ occur, are obtained from the magnitude spectra and are listed in column 4, Table 2. They correspond to corner periods obtained from straight-line approximations of the displacement density spectra, a method used extensively (Hanks and Wyss, 1972; Fletcher et al., 1987) but subjected to similar uncertainties related to the length of the time window as discussed above. Comparison of the magnitude spectra between the three events indicates that the average corner period and the standard deviation of the corner periods, as observed at the 13 stations, are much greater for the Whittier Narrows (WN) earthquake than for the Elmore Ranch (ER) and Superstition Hills (SH) earthquakes. The differences in the corner periods and in the complexities of the spectra apparently indicate some profound differences in the source parameters of the two groups of earthquakes.

Determination of the source parameters

For elastic waves (P- or S-waves) in a homogeneous medium, the velocity amplitude density spectrum $V(f)$ is related to the energy density spectrum $E(f)$ by

$$E(f) = 8\pi \rho_s c_s r^2 V^2(f) \tag{1}$$

where ρ_s and c_s are the density and wave velocity of the given wave type in the material near the source and r is the distance from the source to the point of observation. For P-waves, the energy spectral density of the source $E_p(f)$ is related to the magnitude spectrum $m(f)$ through

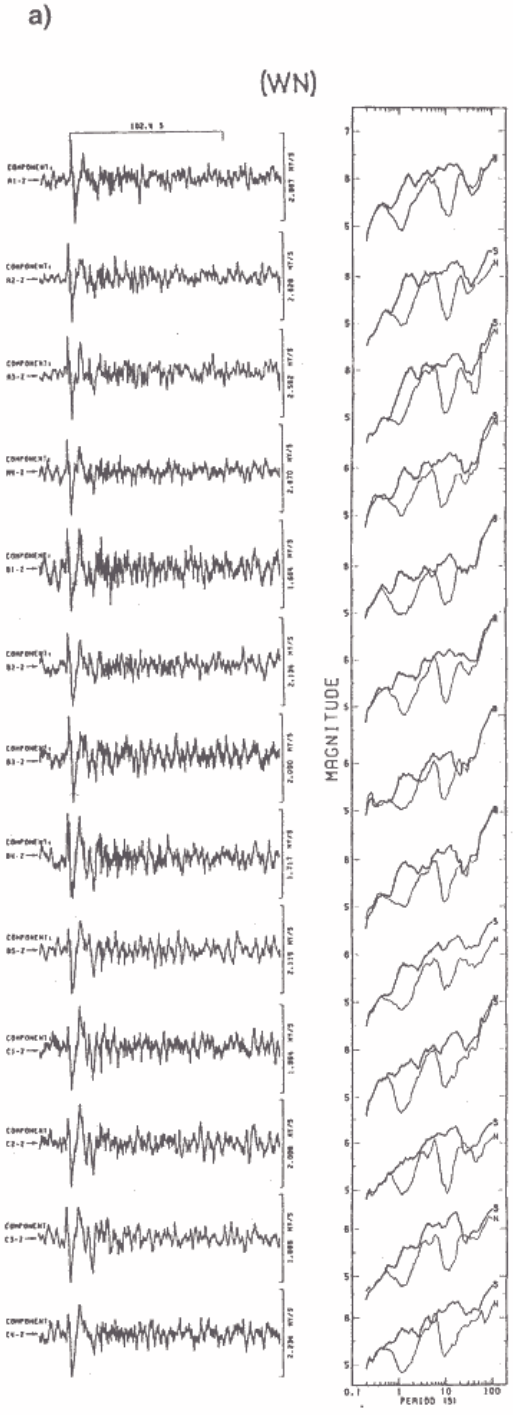

Figure 3 (Continues on the next page). Broadband P-wave signals as recorded at the 13 stations of the GRF array (A1–C4) and corresponding magnitude spectra for the earthquakes listed in Table 1. Note the different magnification for each of the seismograms. For further details see Figure 2. (a) 1 October 1987, 14:42:20 (WN); (b) 24 November 1987, 1:54:14 (ER); (c) 24 November 1987, 13:15:56 (SH).

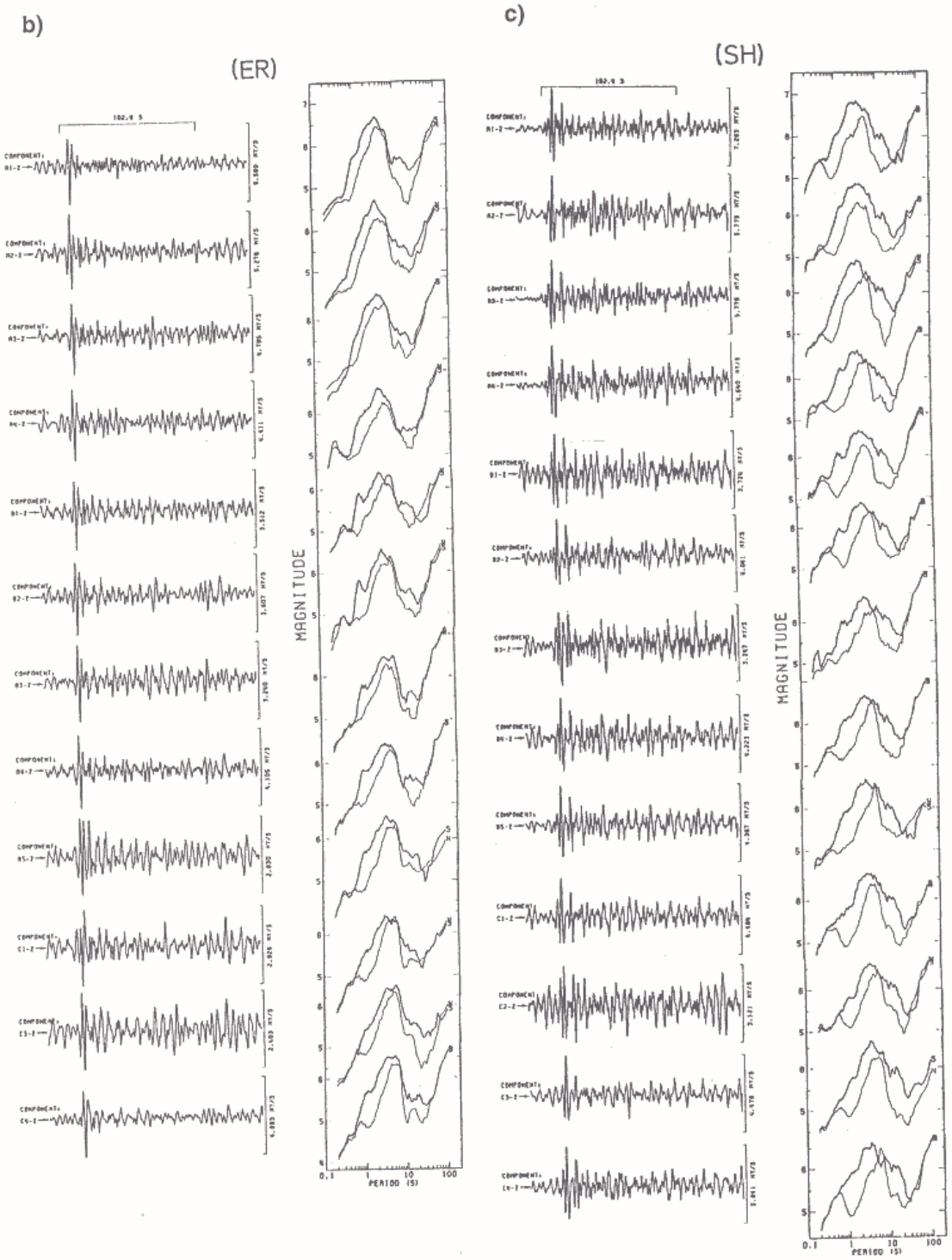
b)
(ER)
c)
(SH)
MAGNITUDE
PERIOD (S)
0.1
1
10
100

Table 2. Source parameters determined from magnitude spectra of the three earthquakes listed in Table 1.

Station GRF	P-wave energy E_P (10^{11} J)	Maximum magnitude, $\hat{m}_f$	Corner period T_o (s)	Parameters based on T_o				Corner period T_c (s)	Parameters based on T_c				Spectral complexity, C
				M_o (10^{17}Nm)	L (km)	D_o (cm)	$\Delta\sigma$ (MPa)		M_o (10^{17}Nm)	L (km)	D_o (cm)	$\Delta\sigma$ (MPa)	
(a)	**1 October, 1987,**			**14:42:20.0**		**(WN)**							
A1	0.79	6.31	17.1	17.2	73.3	2	0.02	6.4	6.4	27.4	6	0.11	2.22
A2	0.64	6.33	17.1	17.9	73.3	3	0.02	4.7	5.0	20.3	9	0.21	1.23
A3	0.61	6.37	17.8	20.6	76.4	3	0.02	6.2	7.2	26.7	8	0.13	1.27
A4	0.63	6.32	12.8	13.4	54.9	3	0.03	5.1	5.3	21.8	8	0.18	1.31
B1	0.47	6.26	12.8	11.5	54.9	3	0.02	4.5	4.1	19.5	8	0.19	1.13
B2	0.40	6.21	12.4	9.9	53.3	3	0.02	5.7	4.6	24.5	6	0.11	1.58
B3	0.44	6.24	13.2	11.4	56.7	3	0.02	7.6	6.6	32.5	5	0.07	1.97
B4	0.52	6.31	12.8	12.9	54.9	3	0.03	6.4	6.4	27.3	6	0.11	1.44
B5	0.52	6.39	17.8	21.9	76.4	3	0.02	9.9	12.2	42.7	5	0.06	1.53
C1	0.38	6.36	17.8	20.2	76.4	3	0.02	7.6	8.6	32.6	6	0.09	1.01
C2	0.43	6.36	16.4	18.5	70.3	3	0.02	7.4	8.3	31.7	6	0.09	1.11
C3	0.36	6.35	16.4	18.4	70.3	3	0.02	9.3	10.4	39.8	5	0.06	1.19
C4	0.48	6.35	17.8	19.7	76.4	3	0.02	10.1	11.2	43.3	4	0.05	1.74
Aver-age:	0.51	6.32	15.6	16.4	66.7	3	0.02	7.0	7.4	30.0	6	0.11	1.44
SD:	0.12	0.05	2.2	3.9	9.6	0.3	0.004	1.8	2.5	7.7	1	0.05	0.34
(b) 24 November 1987				**01:54:14.5**		**(ER)**							
A1	2.8	6.69	3.8	9.3	16.3	26	0.8	3.0	7.5	13.1	33	1.2	0.63
A2	2.8	6.73	3.5	9.5	15.2	31	1.0	3.2	8.5	13.6	34	1.2	0.55
A3	2.3	6.60	3.6	7.1	15.5	22	0.7	3.1	6.1	13.1	27	1.0	0.78
A4	1.9	6.61	3.5	7.1	15.2	24	0.7	3.2	6.4	13.6	26	0.9	0.65
B1	1.1	6.40	3.2	4.0	13.7	16	0.5	3.1	3.9	13.5	16	0.6	1.02
B2	1.3	6.54	3.6	6.2	15.5	19	0.6	3.3	5.7	14.1	21	0.7	0.64
B3	1.3	6.50	6.3	9.9	27.0	10	0.2	3.6	5.7	15.6	18	0.5	0.87
B4	1.2	6.47	3.5	5.1	15.0	17	0.5	2.8	4.1	12.0	21	0.8	0.73
B5	1.3	6.54	3.6	6.2	15.5	19	0.6	3.4	5.9	14.5	21	0.7	0.67
C1	0.8	6.43	3.2	4.2	13.7	17	0.6	3.3	4.4	14.3	16	0.5	0.67
C2													
C3	0.9	6.48	5.9	8.8	25.3	10	0.2	3.9	5.3	16.7	16	0.4	0.67
C4	1.5	6.55	5.3	9.3	22.7	14	0.3	3.6	6.3	15.4	20	0.6	0.77
Aver-age:	1.6	6.55	4.1	7.2	17.6	19	0.6	3.3	5.9	14.1	22	0.8	0.72
SD:	0.7	0.10	1.0	2.0	4.4	6	0.2	0.3	1.3	1.2	6	0.3	0.12
(b) 24 November 1987				**13:15:56.8**		**(SH)**							
A1	7.8	6.84	3.6	12.3	15.4	39	1.2	3.1	10.7	13.4	45	1.6	0.93
A2	6.4	6.76	4.1	11.7	17.6	28	0.8	3.2	9.2	13.9	36	1.2	1.14
A3	5.5	6.78	3.6	10.8	15.5	34	1.0	3.0	8.9	12.8	41	1.5	0.82
A4	4.1	6.65	3.5	7.8	15.0	26	0.8	3.0	6.6	12.7	31	1.1	1.09
B1	3.3	6.62	3.5	7.2	15.0	24	0.7	3.1	6.4	13.4	27	0.9	1.09
B2	2.5	6.60	3.6	7.1	15.5	22	0.7	3.1	6.0	13.2	26	0.9	0.89
B3	2.5	6.00	3.6	7.1	15.5	22	0.7	3.1	6.1	13.4	26	0.9	0.90
B4	3.6	6.86	3.5	12.6	15.0	42	1.3	3.1	7.0	13.1	31	1.1	0.94
B5	3.2	6.68	3.6	8.5	15.5	27	0.8	3.2	7.7	13.9	30	1.0	0.80
C1	3.0	6.63	3.5	7.5	15.2	25	0.8	3.5	7.5	14.9	25	0.8	1.03
C2	2.3	6.62	3.8	7.9	16.3	22	0.6	3.5	7.1	15.0	24	0.7	0.87
C3	2.1	6.65	3.8	8.4	16.3	24	0.7	3.7	8.2	16.0	24	0.7	0.72
C4	2.5	6.62	3.6	7.4	15.5	23	0.7	3.1	6.4	13.2	28	1.0	0.79
Aver-age:	3.8	6.69	3.6	8.9	15.6	28	0.8	3.2	7.5	13.8	30	1.0	0.92
SD:	1.7	0.09	0.2	0.2	0.7	6	0.2	0.2	1.3	0.9	6	0.3	0.13

$$E_p(f) = 10^{2m(f)-1.4} \tag{2}$$

(Nortmann and Duda, 1983). $E_p(f)$ is thereby expressed in J/Hz. By combining (1) and (2) for P-waves we obtain

$$m(f) = \frac{1}{2} \log (8\pi \rho_s c_s r^2) + \log V_p(f) + 0.7 . \tag{3}$$

This formula relates the velocity amplitude density spectrum of far-field P-waves to the P-wave magnitude spectrum of the seismic source. Theoretical spectra predicted by a given source model may be used to determine theoretical magnitude spectra which in turn can be compared with the observed magnitude spectrum of an earthquake. By simultaneous variation of the relevant source parameters, the best match with the observed spectrum can be found.

According to the omega-square model (Aki, 1967; Brune, 1970), the far-field displacement density spectrum of body waves is described by

$$D(f) = \frac{D(\mathrm{O})}{1 + (f/f_c)^2} \tag{4}$$

where f_c is the corner frequency of the source spectrum and $D(\mathrm{O})$ is the value of the flat part of the displacement density spectrum $D(f)$.

Since

$$V(f) = 2\pi f D(f), \tag{5}$$

the far-field velocity amplitude density spectrum of the omega-square model is given by

$$V(f) = \frac{2\pi f D(\mathrm{O})}{1 + (f/f_c)^2} . \tag{6}$$

This function has the maximum at the corner frequency f_c. The value of the flat part of the displacement density spectrum $D(\mathrm{O})$ is proportional to the seismic moment

$$M_o = \frac{4\pi r (\rho_s \rho_r c_r)^{1/2} c_s^{5/2} D(\mathrm{O})}{R_{\theta\phi}} \tag{7}$$

(Aki and Richards, 1980). Here, ρ_r and c_r are the density and wave velocity of the material near the receiver and $R_{\theta\phi}$ is the radiation pattern coefficient. Combining (3), (6) and (7), the magnitude spectrum of the omega-square model is expressed as

$$m(f) = \frac{1}{2} \log\left(\frac{2\pi}{\rho_r\, c_r\, c_s^4}\right) + \log\left(\frac{M_o\, R_{\theta\phi}\, f}{1 + (f/f_c)^2}\right) + 0.7\,. \tag{8}$$

The magnitude spectrum is primarily determined by the seismic moment M_o and the corner frequency f_c. The maximum value of the magnitude spectrum $\hat{m}_f$ is attained at the corner frequency f_c:

$$\hat{m}_f = \frac{1}{2} \log\left(\frac{2\pi}{\rho_r\, c_r\, c_s^4}\right) + \log\left(\frac{M_o\, R_{\theta\phi}\, f_c}{2}\right) + 0.7\,. \tag{9}$$

Rewriting (9), the seismic moment can be calculated knowing $\hat{m}_f$ and the corner period $T_c = 1/f_c$ of the P-wave magnitude spectrum from

$$M_o = (10^{\hat{m}_f - 0.7})\, T_c \left(\frac{2\rho_r\, c_r\, c_s^4}{\pi\, R_{\theta\phi}^2}\right)^{1/2} \tag{10}$$

M_o is expressed in Nm.

Here, c_s and c_r, the P-wave velocities of the material near the source and near the receiver respectively are assumed to be 5800 m/s and 6100 m/s respectively, ρ_r, the density of the material near the receiver, is taken to be 2720 kg m^{-3}, μ, the shear modulus, is assumed to be 2.7×10^{10} Pa, and $R_{\theta\phi}$, the radiation pattern coefficient for P-waves, is taken as 0.44, which is the average value over the focal sphere (Boore and Boatwright, 1984).

The fault length L is approximated by the diameter $2a_o$ of the Brune (1970, 1971) circular fault model ($L = 2a_o$). Thus

$$a_o = 0.37\, c_s/f_c \tag{11a}$$

$$L = 0.74\, c_s T_c \tag{11b}$$

The average displacement D_o is calculated from

$$D_o = \frac{M_o}{\mu\, \pi\, a_o^2} \tag{12}$$

(Aki, 1966), and finally the average static stress drop $\Delta\sigma$ is determined from

$$\Delta\sigma = \frac{7}{16}\frac{M_o}{a_o^3} \tag{13}$$

(Keilis-Borok, 1957).

Earthquakes with complex rupture processes generally have broad and complicated spectra with secondary maxima at periods shorter or longer than T_o, the period at which the maximum magnitude $\hat{m}_f$ occurs (see Fig. 2a). The difficulty in determining the corner periods from such spectra has been discussed by Madariaga (1979), Snoke et al. (1983), Boatwright (1984) and others. Following Duda and Kaiser (1989) three different measures of the corner period are utilized in the present study:

1. T_o, the period at which the maximum magnitude $\hat{m}_f$ occurs, as outlined above. The proximity of secondary maxima at other periods is not taken into account.

2. T_c, the location of the first moment of the energy density spectrum $E_P(f)$ (eq.2) defined as:

$$T_c = \frac{E_P}{\int_0^\infty E_P(f)\, f\, df} \tag{14}$$

where

$$E_P = \int_0^\infty E_P(f)\, df \tag{15}$$

with E_P, being the total P-wave energy radiated from the earthquake focus.

The numerical value for the integrals in equations (14) and (15) is corrected for the energy carried in the signal outside the frequency band considered. The method used to calculate these correction terms has been described by Duda and Kaiser (1989) and earlier by Boatwright and Choy (1986), Snoke (1987), and Di Bona and Rovelli (1988).

3. T_s, determined from

$$T_S = \frac{\pi R_{\theta\phi}\, 10^{2\hat{m}_f - 1.4}}{E_P} \tag{16}$$

(Snoke, 1987; Duda and Kaiser, 1989). Limitations of this method have been discussed by Di Bona and Rovelli (1988).

For an omega-square-spectrum (Aki, 1967; Brune, 1970) T_o, T_c, and T_s are identical. In the case of complex spectra with several maxima, T_c is a weighted average value, the weight of each corner period depending on the energy carried in the respective maximum. Using the first moment of the energy density spectrum (or power spectrum of ground velocity), instead of the first moment of the velocity density spectrum, puts more weight on the largest maximum and therefore shows better agreement with the corner period T_o obtained from visual inspection.

The source parameters are determined individually from the magnitude spectra recorded at the stations of the Graefenberg array. In parallel, source parameters are calculated using T_o, the period where the maximum value of the magnitude spectrum, $\hat{m}_f$, occurs. In this case in equations (10) and (11b) T_c is replaced by T_o. The parameters determined are listed in Table 2 (see also Figure 6).

Interpretation of the magnitude spectrum in terms of the asperity model of the source

A measure of rupture complexity has been proposed by Duda and Kaiser (1989) as

$$C = T_c / T_s \tag{17}$$

where T_c and T_s are defined by equations (14) and (16) respectively. T_s, by definition, is the corner period of a P-wave magnitude spectrum with total P-wave energy E_P and with maximum magnitude $\hat{m}_f$ as determined from the observed spectrum, but with a shape corresponding to an omega-square-displacement spectrum for far field P-waves (Aki, 1967; Brune, 1970). If the observed spectrum complies with the omega-square-spectrum, T_c and T_s are identical and $C = 1$. Earthquakes with complex ruptures radiate comparatively more energy at frequencies above the corner frequency; the spectral falloff toward higher frequencies is more gentle, and consequently T_s is smaller than the corner period T_c, and $C > 1$. This is the case for the magnitude spectrum shown in Figure 2a, where $C = 2.22$ (see Table 2a). The values for the complexity of intermediate to large earthquakes fall in practice in the range $0.5 < C < 2.5$ (Kaiser, 1989). In the following section the complexity factor C is interpreted in terms of an asperity model.

McGarr (1981) assumes the failure of a circular asperity of radius a_i surrounded by a previously faulted annular region of outer radius a_o (Figure 4). Before the seismic event, the annular region $a_i < a < a_o$ has failed under the influence of the ambient faulting stress σ_{af} in either preceding earthquakes or in aseismic creep. The ambient faulting stress σ_{af} is the difference between the regional applied shear stress and the frictional stress that resists

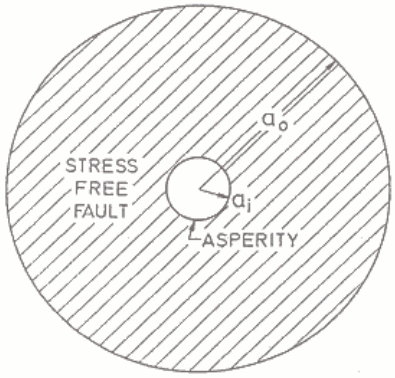

Figure 4. Asperity model adapted from McGarr (1981). The view is normal to the fault plane, where before the event faulting is assumed to have occurred in the hatched annular region. In the faulting process, the asperity with radius a_i fails, followed by a dynamic readjustment of the whole fault plane.

sliding across a fault plane. In the faulting process, the asperity fails with a high stress drop $\Delta\sigma_i$ followed by a dynamic readjustment of the annular fault zone, resulting in a lower stress drop $\Delta\sigma$ throughout the total zone of faulting. The failure of the asperity is associated with the displacement D_i and the large-scale average slip is D_o. The new source parameters can now be determined utilizing equations (8), (9), and (10) of McGarr (1981), which are repeated here with slightly changed notation, and assuming $f(a_i/a_o) = 1.00$ in the original equations, as suggested by McGarr (1981).

$$\sigma_{af} = \frac{2}{3}\Delta\sigma\frac{a_o}{a_i}\left[1 + 0.06\frac{a_i}{a_o} + 0.33\left(\frac{a_i}{a_o}\right)^2 + 0.04\left(\frac{a_i}{a_o}\right)^3\right] \tag{18}$$

$$\Delta\sigma_i = \frac{2}{3}\Delta\sigma\left(\frac{a_i}{a_o}\right)^2 \tag{19}$$

$$D_i = \frac{1.52}{\pi}\frac{\Delta\sigma}{\mu}\frac{a_o^2}{a_i} \tag{20}$$

The radius of the asperity a_i can be determined from the measurement of peak ground velocity $\hat{V}$ and peak acceleration $\hat{A}$ of the far-field S-wave (equations 19, 21, and 25, McGarr, 1981). Equation 25, being the most reliable from both theoretical and observational standpoints according to McGarr (1981), is used in the present study.

To relate the peak ground motion parameters of the far-field S-wave magnitude spectrum to the far-field P-wave magnitude spectrum we assume that the S-wave parameters are proportional to the respective ground motion parameters of the far-field P-wave. As illustrated before, C – the complexity – is a measure of the additional energy radiated at frequencies above the

corner frequency, and therefore reflects the high-frequency ground motion. It is thus related to the peak ground acceleration $\hat{A}$. The rupture of a heterogeneous fault plane (described by asperities, barriers, multiple ruptures, etc.) explains the radiation of additional high-frequency waves (Madariaga, 1983), which generally introduce an f^{-1} decay in the far-field displacement spectrum (Boore and Joyner, 1978). Here we choose a simple spectral model with an intermediate f^{-1} spectral fall-off for the far-field body wave displacement amplitude spectrum at frequencies near the corner frequency as an extension of the Brune (1970) spectrum. A spectrum with this fall-off has been discussed by Madariaga (1976) for his circular fault model and by Stefansson et al. (1979) for earthquakes with uneven rupture propagation or heterogeneous stress distribution. Madariaga (1976) defined three distinct regions in the spectrum, corresponding to the three regions in the present spectral model. Thus, the intermediate frequency region is controlled by the size of the fault. This region also determines the energy of the far-field radiation, since the velocity spectrum is maximum at T_c (equation 14). More recently, Brune et al. (1986) and Priestley et al. (1988) observed the existence of an f^{-1} fall-off for frequencies just above the corner frequency for complex multiple events with incoherent stress release. Choy and Boatwright (1988) observed an intermediate slope in the source spectra of complex earthquakes and interpreted it as an indication that the rupture processes were dominated by the failure of asperities. In terms of the velocity spectrum V(f), this introduces a flat portion with two corner frequencies at $f_c + \Delta f$ and $f_c - \Delta f$, as shown in Figure 5. In this case, the acceleration spectrum, given by

$$A(f) = 2\pi f V(f) \tag{21}$$

has its maximum at the higher corner frequency ($f_c + \Delta f$) (compare with Figure 1 of Joyner, 1984). The relationship between C, Δf, and $A(f)$ is examined in the next section. It must be stressed that the spectrum shown in Figure 5 has been constructed only to find the relation between C and A, and that it is not connected physically to the specific asperity model of McGarr (1981) or any other heterogeneous earthquake source model.

From the definition of C [equations (14), (16), and (17)] it follows that

$$E_P = E_B C \tag{22}$$

where E_P is the total seismic energy determined from the spectrum by equation (15) and E_B is the energy of the theoretical Brune (1970) spectrum $V_B(f)$ in Figure 5. Since the velocity amplitude density spectrum $V(f)$ is related to the energy density spectrum $E(f)$ by equation (1), we can calculate E_B and E_P carried by the theoretical spectra shown in Figure 5 from:

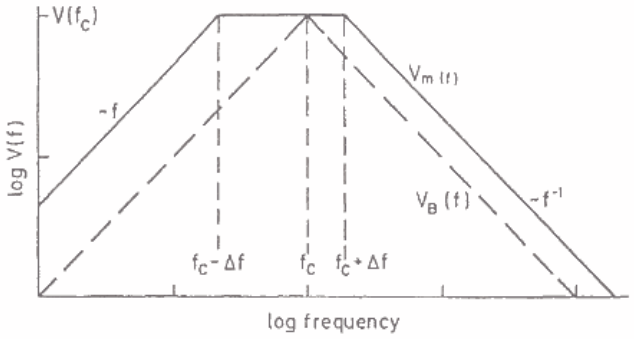

Figure 5. Velocity amplitude spectrum in the far-field for the complex source model shown in Figure 4 and indicated by V_m. V_B (dashed line) corresponds to model of Brune (1970). The corner frequency $f_c = 1/T_c$ is defined by equation (14).

$$E_B = \int_0^\infty E_B(f)\,df = E_B(f_c)\left[\int_0^{f_c}\left(\frac{f}{f_c}\right)^4 df + \int_0^\infty \left(\frac{f_c}{f}\right)^4 df\right] = \frac{8}{15} E_B(f_c)\, f_c \tag{23}$$

$$E_P = \int_0^\infty E_P(f)\,df = E_P(f_c)\left[\int_0^{f_c-\Delta f}\left(\frac{f}{f_c-\Delta f}\right)df + \int_{f_c-\Delta f}^{f_c+\Delta f} df + \int_{f_c+\Delta f}^{\infty}\left(\frac{f_c+\Delta f}{f}\right)df\right] =$$

$$= E_P(f_c)\left[\frac{f_c-\Delta f}{5} + 2\Delta f + \frac{f_c+\Delta f}{3}\right] \tag{24}$$

where from (1)

$$E_P(f_c) = 8\pi\,\rho_s\, c_s\, r^2\, V_P^2(f_c) \tag{25}$$

and from Figure 5

$$E_P(f_c) = E_B(f_c) \tag{26}$$

Inserting (23) and (24) in (22) and considering (26) we obtain:

$$\Delta f = 4 f_c\,(C-1)\,. \tag{27}$$

Thus, knowing C in equation (27) permits us to determine the frequency at which the maximum of the acceleration spectrum $A(f_c + \Delta f)$ in Figure 5 occurs. Since $V(f_c + \Delta f) = V(f_c)$, equations (21) and (27) yield:

$$A(f_c + \Delta f) = 2\pi\, f_c\,(4C - 3)\, V(f_c) \tag{28a}$$

or

$$\frac{V(f_c)}{A(f_c + \Delta f)} = \frac{1}{2\pi f_c (4C - 3)} \tag{28b}$$

Using our assumption that the peak ground parameters of velocity and acceleration are proportional to the respective maximum values of the P-wave velocity and acceleration spectra, *i.e.* $\hat{V} \sim V(f_c)$ and $\hat{A} \sim A(f_c + \Delta f)$, we find:

$$\frac{\hat{V}}{\hat{A}} \sim \frac{1}{f_c (4C - 3)} \tag{29}$$

For P-waves ($c_s = \alpha$), equation (25) of McGarr (1981) results in

$$a_i = \frac{3\,\alpha\,\hat{V}}{\hat{A}} . \tag{30}$$

Considering equations (11a) and (29) and that $a_o \sim \alpha/f_c$, equation (30) becomes:

$$a_i \sim \frac{a_o}{(4C - 3)} \tag{31}$$

Equation (31) in turn permits us to determine the asperity radius a_i from C, except for a proportionality factor. This factor can be derived from the Brune spectrum, *i.e.* for $C = 1$, the value of a_o/a_i is equal to 5.7 (McGarr, 1981). Thus, (31) finally changes to

$$\frac{a_o}{a_i} = 5.7\,(4C - 3) . \tag{32}$$

Equation (32) enables us to calculate a_o/a_i from C for complex earthquakes. For simple earthquakes ($C < 0.80$), we would arrive at an unrealistic result, $(a_o/a_i) < 1$, that is, the asperity radius would exceed the radius of the total faulted area. Thus, the model spectrum (Figure 5) and related assumptions are not adequate for simple-rupture earthquakes. Consequently, for $C > 0.80$ we calculate a_o/a_i from (32) and the additional source parameters σ_{af}, $\Delta\sigma_i$ and D_i from equations (18), (19), and (20) respectively. For $C < 0.8$, however, we simply consider the source as homogeneous, and therefore $\Delta\sigma_i = \Delta\sigma = \sigma_{af}$, and $D_i = D_o$. The additional source parameters are determined on the basis of the array-averaged parameters of Table 2, and the results are displayed in Table 3.

Table 3. Array-averaged source parameters determined from magnitude spectra, considering T_c and C, of the three earthquakes listed in Table 1.

ID	E_P (10^{11}J)	$\hat{m}_f$	T_c (s)	M_o (10^{17}Nm)	L (km)	D_o (cm)	$\Delta\sigma$ (MPa)	C	a_o/a_i	a_i (km)	D_i (cm)	$\Delta\sigma_i$ (MPa)	σ_{af} (MPa)
WN	0.51	6.32	7.0	7.4	30.0	6	0.11	1.44	15.7	0.95	47	18.1	1.2
ER	1.6	6.55	3.3	5.9	14.1	22	0.8	0.72	~1	~7	22	0.8	0.8
SH	3.8	6.69	3.2	7.5	13.8	30	1.0	0.92	3.9	1.78	48	10.0	2.7

Influence of local site conditions

Local geologic conditions in the vicinity of the receiving station can amplify or attenuate the amplitudes of the signals to be studied. To investigate this effect we compare the P-wave signals, magnitude spectra, and source parameters of each earthquake at different stations. All stations of the array are located on homogeneous geological structures in the Swabian-Frankonian Jura (Figure 1b; Harjes and Seidl, 1978).

The signal shape of each earthquake is similar at all stations of the array, but the maximum amplitudes vary by more than a factor of two between different stations (Figure 3). The largest amplitudes are consistently observed at station A1. Frequency-dependent effects are studied more conveniently by comparing the magnitude spectra. Several details in the spectra can be recognized throughout the array: a principal maximum magnitude of 6.3 at a period of 16 s, a broad and complicated spectrum with several secondary maxima at shorter periods (7 s, 4 s, and between 1 and 2 s) for the 1 October Whittier Narrows (WN) earthquake (Figure 3a). The differences between the magnitude spectra are larger at shorter periods, *e.g.* compare the secondary maximum at periods between 1 and 2 s at the northernmost stations A1 and A3 to the same maximum from signals at the southernmost stations C2 and C3 in Figure 3a. This observation illustrates that high-frequency amplitudes are more strongly affected by local site conditions. The characteristic shape of the spectrum, however, remains constant, and is clearly different from the magnitude spectra of the remaining two earthquakes at Elmore Ranch (ER) and Superstition Hills (SH) (Figure 3b, c). Clear differences in the magnitude spectra of the 1 October earthquake (WN) on one side and of the 24 November earthquakes (ER and SH) on the other can be recognized uniformly at all stations of the array (Fig. 3). From Table 2 and Figure 6 further conclusions may be drawn regarding the influence of local site conditions. The P-wave energy of each earthquake is found generally to be largest for subarray A and smallest for subarray C. This fact is in agreement with the assumption of a regional decrease of Q values in the N–S direction underneath the array. The differences can be up to a factor of four between stations A1 and C3. The value

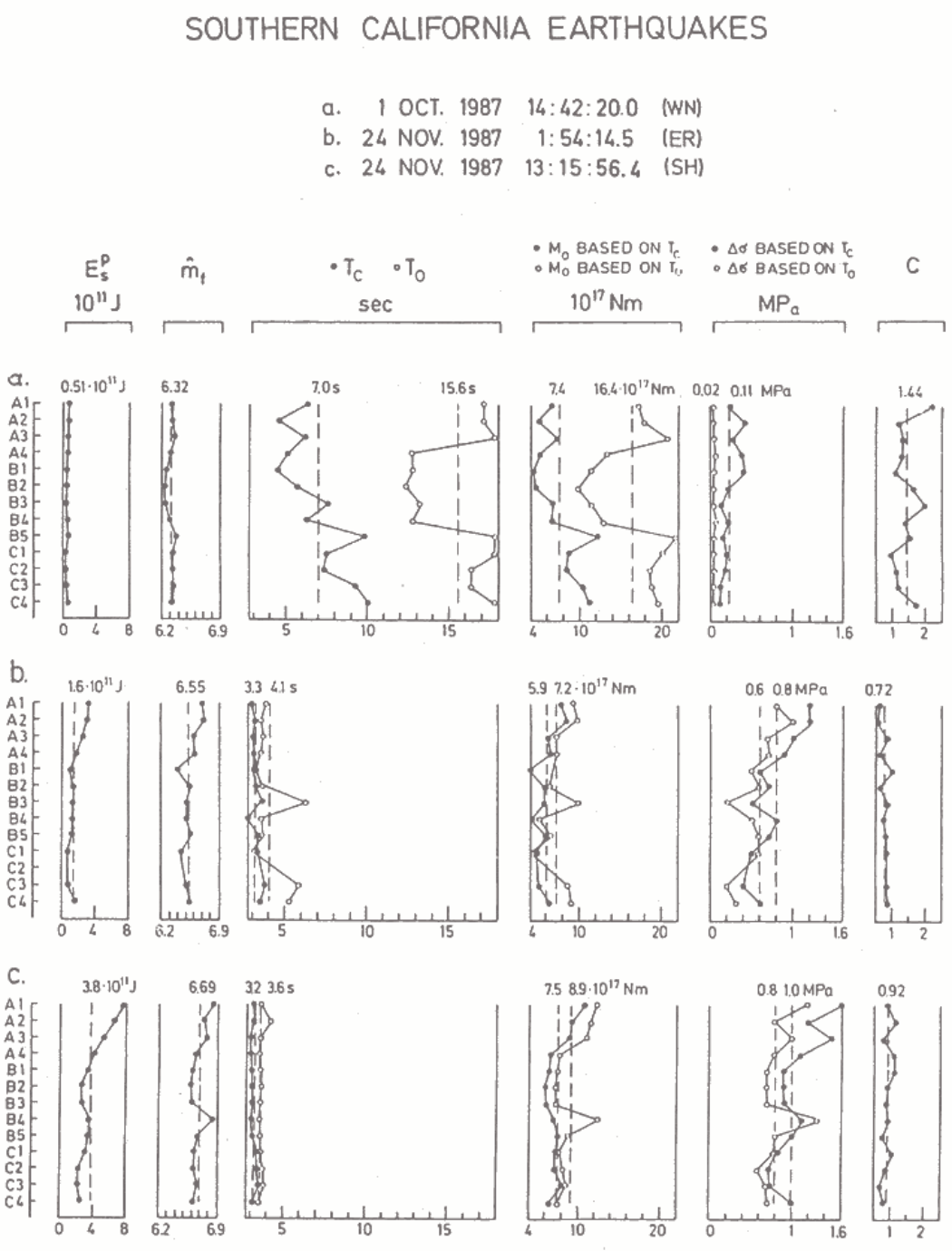

Figure 6. Source parameters determined from magnitude spectra (Figure 3) at the 13 stations (A1–C4) as listed in Table 2. The arithmetic mean over all stations of the array is indicated by a vertical dashed line with the value displayed at the upper end.

of the maximum spectral magnitude however reveals a remarkable stability at the stations of the array, with a standard deviation of only 1%.

The corner periods T_c and T_o for the earthquakes of 24 November (ER and SH) are similar, T_c being generally smaller, and fairly stable throughout the array. For the 1 October earthquake (WN), T_o is more than twice as large as T_c, and there is a considerable amount of scatter, both in T_c and T_o. This signifies not only that the determination of the corner period of broad complex spectra is difficult if only one station is used, but, in addition, that such corner periods are more affected by near-station-conditions than those of simple spectra. In all cases, however, the amount of scatter is smaller for T_c than for T_o. The relatively high stability of T_c results from the integration of the spectrum. The respective advantage of using integrals of spectra has been pointed out earlier by Boatwright (1980), Hanks (1982), Snoke et al. (1983), and Andrews (1986).

The absolute values of seismic moment and the stress drop are dependent on the way the corner period is determined in practice, and therefore subjected to the same uncertainties as the corner period itself. This drawback does not apply to the relative values of the parameters if determined in one and the same way, especially if the values are determined as array-averages. The parameters based on T_c show less scatter and appear to have more realistic values (Table 2). The standard deviation from the mean for each event is 17–34% for M_o, 6–26% for L, 17–27% for D, and 30–45% for $\Delta\sigma$.

The complexity shows no obvious correlation with any other source parameter nor any systematic dependence on the location of the station (Figure 6). Different conditions near the station seem to have only minor effects on this measure of source complexity.

Comparison and interpretation of source parameters

The average values of the source parameters determined from the Gräfenberg (GRF) broadband array for the three events are presented in Table 3. The seismic moments determined in the present study are compared in Table 4 with results obtained by other investigators through different analytical techniques and utilizing different data sources. The seismic moments published in the Preliminary Determination of Epicenters (NEIC) are determined from long-period body waves using the moment tensor inversion method described by Sipkin (1982). However, a different teleseismic data set and a time-dependent moment-tensor algorithm were used by Sipkin (1989) for the Elmore Ranch (ER) and Superstition Hills (SH) earthquakes. Agnew and Wyatt (1989) obtained estimates of the moments from the strain/tilt data, whereas Bent et al. (1988, 1989) and Frankel and Wennerberg (1988, 1989) utilized long-period body wave data and strong-motion accelerograms for the ER and SH events. Regional broadband data were used by Bolt et al. (1989);

Table 4. Comparison of seismic moments determined in various studies

(a) 1 October 1987, Whittier Narrows (WN) Earthquake

Investigators	M_o ($\times 10^{17}$Nm)
Barker (1988)	7.4
Bent and Helmberger (1989)	12.0
Bolt et al. (1989)	10.0
Hartzell and Iida (1990)	7.4 to 10.0
Lin and Stein (1989)	10.0
Linde and Johnston (1989)	6.7
NEIC (1987)	8.4
Present Study	7.4

(b) 24 November 1987, Elmore Ranch (ER) and Superstition Hills (SH) Earthquakes

	M_o ($\times 10^{17}$Nm)	
Investigators	ER	SH
Agnew and Wyatt (1989)	7.5	32 to 63
Bent et al. (1989)	27.0	36 to 72
Frankel and Wennerberg (1989)	–	14
NEIC (1987)	9.1	62
Sipkin (1989)	23	100
Present Study	5.9	7.5

short- and long-period data were utilized by Bent and Helmberger (1989), and geodetic elevation changes were employed by Lin and Stein (1989) for the Whittier Narrows (WN) earthquake.

The seismic moment of 7.4×10^{17} Nm estimated by us for WN is identical with the result obtained by Barker (1988) and agrees well with the values obtained by Hartzell and Iida (1990) and Linde and Johnston (1989) and NEIC (1987), but is slightly lower than the value of 10×10^{17} Nm obtained by Bolt et al. (1989) and Lin and Stein (1989). The result obtained by Bent and Helmberger (1989) is only 1.6 times our estimate of the seismic moment. Further, Barker's (1988) waveform inversion yields moment tensors with large non-double couple component, about 30 to 50% of a pure double couple. Such a large deviation can be indicative of a complex, multiple rupture process (Dziewonski and Woodhouse, 1983; Hinzen, 1986; and Sipkin, 1986). In fact Bent and Helmberger (1989) concluded from a long- and short-period body waveform study that the WN main shock consisted of two subevents, the second occurring 1 s later and 3 km shallower than the first. Hartzell and Iida (1990) inverted strong motion data of WN and obtained a complex rupture process with separate concentrations of slip, the major source having a radius of 2–3 km and a slip of 55–90 cm. Their results are in good agreement with ours with asperity radius of a_i = 0.95 km and slip over asperity, d_i = 47 cm. The multiple ruptures within the focal zone during a short interval undoubtedly make the radiated energy complex as indicated by the high value of the complexity factor C for the WN earthquake.

Strong-motion recordings of the Elmore Ranch and the Superstition Hills earthquakes analyzed by Frankel and Wennerberg (1988, 1989) and Wald and Somerville (1988), as well as the comparison of teleseismic waveforms by Bent et al. (1988, 1989), indicate a simple, uniform rupture for ER and a complex, multiple rupture for SH. The C-values determined in this study agree well with these observations. Wald and Somerville (1988) explain this difference in complexity by the fact that SH ruptured through a geologically more complex region. As a result of this complexity, the value for a_o/a_i is four times greater for SH, and the local stress drop $\Delta\sigma_i$ is larger by a factor of 10 for SH if compared to ER, though the average stress drop $\Delta\sigma$ is similar for these two events. According to McGarr (1981) $\Delta\sigma_i$ represents the highest localized stress drop measured within a faulted region. The largest estimate for $\Delta\sigma_i$ is obtained for WN (18 MPa), although this event has by far the lowest average stress drop $\Delta\sigma$ (0.1 MPa).

Though similar in magnitude, WN and ER are two extremely different earthquakes. WN is a very complex event with a local stress drop more than two orders of magnitude higher than the average stress drop over the fault, whereas ER is the result of a smooth, simple rupture with a homogeneous stress drop. The relative asperity size a_o/a_i and the localized stress drop $\Delta\sigma_i$ mainly reflect the nonuniform distribution of various physical properties on the fault plane, which Papageorgiou and Aki (1983) summarily call the inhomogeneity of the fault.

As seen in Table 3, the average stress drop $\Delta\sigma$ does not reflect the level of the regional stress field for complex events. The ambient faulting stress, σ_{af}, determines the level of stress accumulation within a seismogenic province (McGarr, 1981), and represents the assumed regional level of shear stress that can cause displacement along a fault. It is interesting to note that σ_{af} for SH is three times the value for ER, although both events occur in the same region. There are several possible explanations:

1. A temporal increase in the level of the regional stress field occurred within the 12 hours between the two shocks. Given and Stuart (1988) and Hudnut et al. (1989) provided convincing evidence that the rupture of SH was triggered by a stress field change caused by ER.
2. The frictional stress resisting fault slip is higher at the fault that ruptured in SH. This could be the consequence of the fact mentioned before, that this fault is geologically more complex.
3. The stress field has a higher level in the NW–SE than in the NE–SW direction.
4. The value of σ_{af} for SH is possibly erroneous because the GRF array is near nodal for this event.

It is difficult to determine which of the four explanations is the most plausible.

On the basis of Table 3 as well as from Figures 2 and 6, we divide the earthquakes investigated in two groups. The earthquake at Whittier Narrows (WN) is characterized by a high rupture complexity with an extremely inhomogeneous stress drop compared to the Elmore Ranch (ER) and the Superstition Hills (SH) earthquakes. The focal mechanism by NEIC of WN corresponds to thrust faulting with a moderate strike-slip component, whereas ER and SH are both strike-slip events. This fact also suggests a different tectonic environment in the two regions. Regional variations in stress drop and apparent stress for Southern California earthquakes have been reported, by among others, Wyss and Brune (1971), Thatcher and Hanks (1973), and Fletcher et al. (1987). Estimates of the complexity C and related earthquake source parameters should supplement such observations.

Conclusions

The main results derived from the analysis of broadband seismograms from the GRF array for the three major 1987 Southern California earthquakes are:

1. P-wave magnitude spectra can be determined fairly reliably at a single station. The magnitude spectrum is more affected by local site conditions at shorter periods. This can explain the remarkable stability of the maximum magnitude at longer periods with an uncertainty of less than 0.1 magnitude units.
2. A method for routine determination of other source parameters such as the seismic moment, the energy, the average stress drop, and the ambient faulting stress from the P-wave magnitude spectra yields reliable estimates of these parameters, provided the station is not near a nodal plane.
3. The most significant difference between the three earthquakes investigated rests in the rupture complexity C. The earthquake at Whittier Narrows reveals a high value for C, whereas the Elmore Ranch and Superstition Hills earthquakes have low to intermediate C-values. The complexity C and the ambient faulting stress σ_{af} are useful parameters describing the inhomogeneity of a fault and assessing the relative level of stress accumulation within a seismogenic region. Because the complexities on a fault are the main source of the high-frequency waves generated during earthquake faulting (Madariaga, 1983; Heaton and Hartzell, 1988), estimating C for an earthquake fault will be essential for the prediction of strong motion. Regions with high levels of stress accumulation might indicate the location of future large earthquakes. Thus, observations of the regional and temporal distribution of the ambient faulting stress could be relevant to the problem of earthquake prediction.

Acknowledgements – The study was supported by the Deutsche Forschungsgemeinschaft, Bonn, F. R. Germany. One of the authors (D. K. C.) was the recipient of a scholarship under the partnership program between Hamburg University and Indiana University. All support is gratefully acknowledged.

References

Agnew, D.C. and F. K. Wyatt (1989): The 1987 Superstition Hills earthquake sequence: Strains and tilts at Piñ Flat Observatory. Bull. Seism. Soc. Am., **79**, 480–492.

Aki, K. (1966): Generation and propagation of G-waves from the Niigata earthquake of June 16, 1964. Bull. Eathquake Res. Inst., **44**, 23–88.

Aki, K. (1967): Scaling law of seismic spectrum. J. Geophys. Res., **72**, 1217–1231.

Aki, K. and P. G. Richards (1980): Quantitative Seismology. Freeman, San Francisco.

Andrews, D. J. (1986): Objective determination of source parameters and similarity of earthquakes of different size. *In:* S. Das, J. Boatwright, and C. H. Scholz (Eds.), Earthquake source mechanics. Geophysical Monograph 37, Maurice Ewing, **6**, Geophys. Un., Wash. D. C., 259–267.

Barker, J. S. (1988): A teleseismic body wave analysis of the October 1, 1987 Whittier Narrows earthquake. Seism. Res. Let., **59**, 4.

Båth, M., (1974): Spectral analysis in geophysics. Elsevier, Amsterdam-Oxford-New York.

Bent, A. L. and D. V. Helmberger (1989): Source complexity of the October 1, 1987, Whittier Narrows earthquake. J. Geophys. Res., **94**, 9548–9556.

Bent, A. L., P. Ho-Liu, and D. V. Helmberger (1988): The November 1987 Superstition Hills earthquake and comparisons with previous neighbaring events. Seism. Res. Let., **59**, 49.

Bent, A. L., D. V. Helmberger, R. J. Stead, and P. Ho-Liu (1989): Waveform modeling of the November 1987 Superstition Hills earthquakes. Bull. Seism. Soc. Am., **79**, 500–514.

Berckhemer, H. (1971): The concept of wide band seismometry. Observ. Royal Belgique, Serie Geophysique No. 101, 214–220.

Boatwright, J. (1980): A spectral theory for circular seismic sources; simple estimates of source dimension, dynamic stress drop, and radiated seismic energy. Bull. Seism. Soc. Am., **70**, 1–27.

Boatwright, J. (1984): The effect of rupture complexity on estimates of source size. J. Geophys. Res., **89**, 1132–1146.

Boatwright, J. and G. L. Choy (1986): Teleseismic estimates of the energy radiated by shallow earthquakes. J. Geophys. Res., **91**, 2095–2112.

Bolt, B. A., A. Lomax, and R. A. Uhrhammer, (1989): Analysis of regional broadband recordings of the 1987 Whittier Narrows, California, earthquake. J. Geophys. Res., **94**, 9557–9568.

Boore, D. M. and J. Boatwright (1984): Average body-wave radiation coefficients. Bull. Seism. Soc. Am., **94**, 1615–1621.

Boore, D. M. and W. B. Joyner, (1978): The influence of rupture incoherence on seismic directivity. Bull. Seism. Soc. Am., **68**, 283–300.

Brune, J. N. (1970): Tectonic stress and the spectra of seismic shear waves from earthquakes. J. Geophys. Res., **75**, 4997–5009.

Brune, J. N, (1971): Correction. J. Geophys. Res., **76**, 5002.

Brune, J. N., J. Fletcher, F. Vernon, L. Haar, T. Hanks, and J. Berger (1986): Low stress-drop earthquakes in the light of new date from the Anza, California telemetered digital array. In: S. Das, J. Boatwright and C. H. Scholz (Editors), Earthquake source mechanics. Geophysical Monograph 37, Maurice Ewing, **6**, Am. Geophys. Un., Wash. D. C., 237–245.

Chowdhury, D. K. and S. J. Duda (1986): Broadband seismograms, band-pass seismograms, and spectral magnitudes for a selection of 1979, 1980, and 1981 earthquakes. Institut für Geophysik, Universität Hamburg, 180 pp.

Choy, G. L. and J. Boatwright (1988): Teleseismic and near-field analysis of the Nahanni earthquakes in the Northwest Territories, Canada. Bull. Seism. Soc. Am., **78**, 1627–1652.

Di Bona, M. and A. Rovelli (1988): Effects of the bandwidth limitation on stress drops estimated from integrals of the ground motion. Bull. Seism. Soc. Am., **78**, 1818–1825.

Duda, S. J., and D. Kaiser (1989): Spectral magnitudes, magnitude spectra, and earthquake quanitification: The stability issue of corner period and of the maximum magnitude for a given earthquake. Tectonophysics, **166**, 205–219.

Dziewonski, A. M. and J. H. Woodhouse (1983): An experiment in systematic study of global seismicity: Centroid-moment tensor solutions for 201 moderate and large earthquakes of 1981. J. Geophys. Res., **88**, 3247–3271.

Fletcher, J., K. Haar, T. Hanks, L. Baker, F. Vernon, J. Berger, and J. Brune (1987): The digital array at Anza, California: Processing and initial interpretation of source parameters. J. Geophys. Res., **92**, 369–382.

Frankel, A. and L. Wennerberg (1988): Rupture process of the November 24, 1987 Superstition Hills earthquake determined from strong motion recordings. Seism. Res. Let., **59**, 48.

Frankel, A. and L. Wennerberg (1989): Rupture process of the M_s 6.6 Superstition Hills earthquake determined from strong-motion recordings: Application of tomographic source inversion. Bull. Seism. Soc. Am., **79**, 515–541.

Given, D. D. and W. D. Stuart (1988): A fault interaction model for triggering of the Superstition Hills earthquake of November 24, 1987. Seism. Res. Let., **59**, 48.

Gutenberg, B. and C. F. Richter (1956): Magnitude and energy of earthquakes. Ann. Geofis., **9**, 1–15.

Hamilton, R. M. (1972): Aftershocks of the Borrego Mountain earthquake from April 12 to June 12, 1968, in the Borrego Mountain earthquake of April 9, 1968. U. S. Geol. Surv. Profess. Paper 787, 31–54.

Hanks, T. C. (1982): Reply to »Comments on 'The corner frequency shift, earthqauke source models, and Q.'«. Bull. Seism. Soc. Am., **72**, 1433–1445.

Hanks, T. C. and C. R. Allen (1989): The Elmore Ranch and Superstition Hills earthquakes of 24 November 1987: Introduction to the special issue. Bull. Seism. Soc. Am., **79**, 231–238.

Hanks, T. C. and M. Wyss (1972): The use of body-wave spectra in the determination of seismic-source parameters. Bull. Seism. Soc. Am., **62**, 561–589.

Harjes, H. F. and D. Seidl (1978): Digital recording and analysis of broad-band seismic data at the Gräfenberg (GRF)-Array. J. Geophys., **44**, 511–523.

Hartzell, S. H. and M. Iida (1990): Source complexity of the 1987 Whittier Narrows, California, earthquake from the inversion of strong motion records. J. Geophys. Res., **95**, 12475–12485.

Heaton, T. H. and S. H. Hartzell (1988): Earthquake ground motions. Ann. Rev. Earth Planet. Sci., **16**, 121–145.

Hinzen, K. G. (1986): Comparison of fault-plane solutions and moment tensors. J. Geophys., **59**, 112–118.

Hudnut, K. L., L. Seeber, T. Rockwell, J. Goodmacher, R. Klinger, S. Lindvall, and R. McElwain (1989): Surface ruptures on cross-faults in the 24 November 1987 Superstition Hills earthquake sequence, California. Bull. Seism. Soc. Am., **79**, 282–296.

Johnson, C. E. and L. K. Hutton, (1982): Aftershocks and preearthquake seismicity, in the imperial Valley, California, earthquake of October 15, 1979: U. S. Geol. Surv. Profess. Paper 1254, 59–76.

Joyner, W. B. (1984): A scaling law for the spectra of large earthquakes. Bull. Seis. Soc. Am., **74**, 1167–1188.

Kaiser, D. (1989): Seismizität des Erdkörpers: Magnitudenspektren und andere Erdbeben-Herdparameter aufgrund von Breitband-Seismogrammen. Ph.D.-Thesis, Universität Hamburg.

Kaiser, D. and S. J. Duda (1986): Broadband seismograms, band-pass seismograms, and spectral magnitudes for a selection of 1978 earthquakes. Institut für Geophysik, Universität Hamburg, 61 pp.

Kaiser, D. and S. J. Duda (1988): Magnitude spectra and other source parameters for some major 1985 and 1986 earthquakes. *In:* O. Kulhánek (Ed.), Seismic source physics and earthquake prediction research. Tectonophysics, **152**, 303–318.

Keilis-Borok, V. (1957): On estimation of the displacement in an earthquake source and of source dimensions. Ann. Geofis., **12**, 205–214.

Lin, J. and R. S. Stein (1989): Coseismic folding, earthquake recurrence, and the 1987 source mechnism at Whittier Narrows, Los Angeles basin, California. J. Geophys. Res., **94**, 9614–9632.

Linde, A. T. and M. J. S. Johnston (1989): Source parameters of the October 1, 1987 Whittier Narrows earthquake from crustal deformation data. J. Geophys. Res. **94**, 9633–9643.

Madariaga, R. (1976): Dynamics of an expanding circular fault. Bull. Seism. Soc. Am., **66**, 639–666.

Madariaga, R. (1979): On the relation between seismic moment and stress drop in the presence of stress and strength heterogeneity. J. Geophys. Res., **84**, 2244–2250.

Madariaga, R. (1983): High frequency radiation from dynamic earthquake fault models. Ann. Geophys., **1**, 17–24.

McGarr, A. (1981): Analysis of peak ground motion in terms of a model of inhomogeneous faulting. J. Geophys. Res., **86**, 3901–3912.

Nortmann, R. and S. J. Duda (1982): The amplitude spectra of p-and s-waves and the body-wave magnitude of earthquakes. Tectonophysics, **84**, 17–32.

Nortmann, R. and S. J. Duda (1983): Determination of spectral properties of earthquakes from their magnitude. Tectonophysics, **93**, 251–275.

Papageorgiou, A. S. and K. Aki (1983): A specific barrier model for the quantitative description of inhomogeneous faulting and the prediction of strong ground motion. I. Description of the model. Bull. Seism. Soc. Am., **73**, 693–722.

Priestley, K. F., K. D. Smith, and R. S. Cockerham (1988): The 1984 Round Valley, California earthquake sequence. Geophys. J., **95**, 215–235.

Sarkar, D. and S. J. Duda (1985): Spectral P-wave magnitudes, Aki's omega-square model and source parameters of earthquakes. Tectonophysics, **188**, 175–193.

Savino, J., K. McCamy, and G. Hade (1972): Structures in earth noise beyond twenty seconds – A window for earthquakes. Bull. Seism. Soc. Am., **62**, 141–176.

Sipkin, S. A. (1982): Estimation of earthquake source parameters by the inversion of waveform data: Synthetic seismograms. Phys. Earth Planet. Inter., **30**, 242–259.

Sipkin, S. A. (1986): Interpretation of non-double-couple earthquake source mechanisms derived from moment tensor inversion. J. Geophys. Res., **91**, 531–547.

Sipkin, S. A. (1989): Moment-tensor solutions for the 24 November 1987 Superstition Hills, California, earthquakes. Bull. Seism. Soc. Am., **79**, 493–499.

Snoke, J. A. (1987): Stable determination of (Brune) stress drops. Bull. Seism. Soc. Am., **77**, 530–538.

Snoke, J. A., A. T. Linde, and I. S. Sacks (1983): Apperent stress: an estimate of the stress drop. Boll. Seism. Soc. Am., **73**, 339–348.

Stefánsson, R., I. S. Sacks, and A. T. Linde (1979): Stress field changes during a tectonic episode in northern Iceland. Carnegie Inst. Wash. Year Book **78**, 320–325.

Thatcher, W. and T. C. Hanks (1973): Source Parameters of Southern California earthquakes. J. Geophys. Res., **78**, 8547–8576.

Tucker, B. E. and Brune, J. N., 1977. Source mechanism and m_b–M_s analysis of aftershocks of the San Fernando earthquake. Geophys. J. R. Astron. Soc., **49**, 371–426.

Wald, D. J. and P. G. Somerville (1988): Simulation of accelerograms of the 1987 Superstition Hills earthquake sequence. Seism. Res. Let., **59**, 49.

Wyss, M. and J. N. Brune (1971): Regional variations of source properties in Southern California estimated from the ratio of short to long period amplitudes. Bull. Seism. Soc. Am., **61**, 1153–1168.

Corresponding autor's address: Dr. Diethelm Kaiser, Institute of Geophysics, Hamburg University, Budesstraße 55, 20146 Hamburg, F. R. Germany